

# Quantum Simulation of Helium Hydride in a Solid-State Spin Register

Ya Wang,<sup>1</sup> Florian Dolde,<sup>1</sup> Jacob Biamonte,<sup>2,\*</sup> Ryan Babbush,<sup>3,4</sup> Ville Bergholm,<sup>2</sup> Sen Yang,<sup>1</sup> Ingmar Jakobi,<sup>1</sup> Philipp Neumann,<sup>1</sup> Alán Aspuru-Guzik,<sup>3</sup> James D. Whitfield,<sup>5</sup> and Jörg Wrachtrup<sup>1,†</sup>

<sup>1</sup>*3rd Institute of Physics, Research Center Scope and IQST,  
University of Stuttgart, 70569 Stuttgart, Germany*

<sup>2</sup>*ISI Foundation, Via Alassio 11/c, 10126 Torino, Italy*

<sup>3</sup>*Department of Chemistry and Chemical Biology,  
Harvard University, Cambridge, MA 02138 USA*

<sup>4</sup>*Google, 150 Main Street, Venice Beach, CA 90291, USA*

<sup>5</sup>*Vienna Center for Quantum Science and Technology, University of Vienna,  
Department of Physics, Boltzmannngasse 5, Vienna, Austria 1090*

(Dated: May 13, 2014)

*Ab initio* computation of molecular properties is one of the most promising applications of quantum computing. While this problem is widely believed to be intractable for classical computers, efficient quantum algorithms exist which have the potential to vastly accelerate research throughout in fields ranging from material science to drug discovery. Using a solid-state quantum register realized in a nitrogen-vacancy (NV) defect in diamond, we compute the bond dissociation curve of the minimal basis helium hydride cation,  $\text{HeH}^+$ . Moreover, we report an energy uncertainty (given our model basis) of the order of  $10^{-14}$  Hartree, which is ten orders of magnitude below desired chemical precision. As NV centers in diamond provide a robust and straightforward platform for quantum information processing, our work provides several important steps towards a fully scalable solid state implementation of a quantum chemistry simulator.

Quantum simulation, as proposed by Feynman [1] and elaborated by Lloyd [2] and many others [3–7], exploits the inherent behavior of one quantum system as a resource to simulate another quantum system. Indeed, there have been several experimental demonstrations of quantum simulators in various architectures including quantum optics, trapped ions, and ultracold atoms [8]. The importance of quantum simulators applied to electronic structure problems has been detailed in several recent review articles including [9–14] and promises a revolution in areas such as materials engineering, drug design and the elucidation of biochemical processes.

The computational cost of solving the full Schrödinger equation of molecular systems using any known method on a classical computer scales exponentially with the number of atoms involved. However, it has been proposed that this calculation could be done efficiently on a quantum computer, with the cost scaling linearly in propagation time [6]. There is now a growing body of work proposing efficient quantum simulations of chemical Hamiltonians, e.g. [15–22]. A general procedure to obtain molecular eigenenergies to a desired precision is: (*i*) mapping molecular wave functions into the computational basis, (*ii*) preparing the quantum simulator into an ansatz state which is close to an eigenstate of the simulated Hamiltonian  $H_{\text{sim}}$ , (*iii*) encoding the energies into a relative phase by simulating the time evolution operator  $e^{-itH_{\text{sim}}/\hbar}$  using quantum gates, and (*iv*) extracting the energies to desired precision using a variant of the quantum phase estimation algorithm [2, 15, 23] or, more recently, compressive sensing algorithms [24]. Experimental realizations of the quantum simulation of electronic structure began with the simulation of molec-

ular hydrogen using quantum optics [16] and liquid state NMR [25]. Chemical simulation of reaction dynamics on an eight-site lattice was then performed in NMR [26]. A calculation of the energy of the helium hydride cation in a photonics setup using a quantum variational eigensolver that avoids phase estimation has also been performed [27].

Nitrogen-vacancy (NV) centers in diamond offer a scalable and precise platform for quantum simulation which does not suffer from signal losses as the system size increases, and can avoid challenges such as the need for post-selected measurements. Progress to date has shown that such systems are among the most accurate and most controllable candidates for quantum information processing [28–39]. Milestone demonstrations include high-fidelity initialization and readout [28–31], on-demand generation of entanglement [31–36], implementation of quantum control [36, 40, 41], ultra-long spin coherence time [38], non-volatile memory [39], quantum error correction [31, 37], as well as a host of metrology and sensing experiments [42, 43]. Several proposals to scale up the size of NV systems currently exist, e.g. [36, 44]. Building on this premise, this is the first study reporting the use of a solid state spin system to simulate quantum chemistry.

The chemical system we consider in this paper is the helium hydride cation,  $\text{HeH}^+$  (see Fig. 1a), believed to be the first molecule in the early universe [45]. While  $\text{HeH}^+$  is isoelectronic (i.e. has the same number of electrons) with the previously studied molecular hydrogen, the reduced symmetry requires that we simulate larger subspaces of the full configuration interaction (FCI) Hamil-

tonian  $H_{\text{sim}}$ . Specifically, we consider

$$H_{\text{sim}} = T_e + W_{ee} + V_{eN}(R) + E_N(R) \quad (1)$$

in a minimal single particle basis with one site per atom. Here,  $T_e$  and  $W_{ee}$  are the kinetic and Coulomb operators for the electrons,  $V_{eN}$  is the electron-nuclear interaction, and  $E_N$  is the nuclear energy due to the Coulomb interaction between the hydrogen and helium atoms. The last two terms depend on the internuclear distance  $R$ .

In this work, we consider the singlet ( $S = 0$ ) sector of the electronic Hamiltonian in a minimal single-electron basis consisting of a single site at each atom given by contracted Gaussian orbitals. After taking symmetries into account, the Hamiltonian can be represented as a  $3 \times 3$  matrix in the basis  $(\Psi_1, \Psi_6, \frac{1}{\sqrt{2}}(\Psi_3 - \Psi_4))$  (see Methods). Each term of the Hamiltonian in the single particle basis (e.g.  $\langle \chi_i | (T_e + V_{eN}) | \chi_j \rangle$ ) is precomputed classically at each internuclear separation  $R$  using the canonical spin orbitals found via the Hartree-Fock (HF) procedure which often scales as a third order polynomial in the number of basis functions.

After obtaining  $H_{\text{sim}}$  through this (typically) efficient classical computation, we perform the quantum simulation of this molecule on a single-NV register, which consists of an electronic spin-1 and an associated  $^{14}\text{N}$  nuclear spin-1 forming a qutrit pair (see Fig. 1b). The electronic spin-1 of the NV system acts as the *simulation register* through mapping the molecular basis  $(\Psi_1, \Psi_6, \frac{1}{\sqrt{2}}(\Psi_3 - \Psi_4))$  onto its  $m_s = (1, 0, -1)$  states. The  $^{14}\text{N}$  nuclear spin-1 is used as the *probe register* to read out the energies using the iterative phase estimation algorithm (IPEA) [46], as shown in Fig. 1c.

The controlled evolution  $e^{-itH_{\text{sim}}}$  (we set  $\hbar = 1$  from now) on the electron spin is implemented using optimal control theory, which helps to realize the most precise simulation of quantum chemistry to date. Without post-selection and at room temperature, our experimentally computed energy agrees with the corresponding classical calculations to within chemical precision, with a deviation of  $1.4 \times 10^{-14}$  Hartree. By performing the simulation process for different values of  $R$ , the electronic potential energy surfaces are also experimentally obtained.

In order to efficiently sample the eigenenergy  $E_n$  as the size of the system grows, one must prepare an ansatz state that has an overlap with the corresponding eigenstate  $|e_n\rangle$  that decreases at most polynomially in the system size. The phase estimation algorithm [23] can then be used to project the ansatz state into the exact eigenstate with sufficiently high probability. One possible approach to realize this requirement is to use adiabatic state preparation [15, 25, 47], the performance of which depends on the energy gap during the entire evolution process. An alternative approach is to approximate the eigenstate with a trial state. Such trial states can often be prepared based on classical approximate methods. In

our case, the simulation register is initialized in a trial state  $|\tau\rangle \in \{|+1\rangle, |-1\rangle\}$ , expressible as a superposition of all the  $H_{\text{sim}}$  eigenstates,  $|\tau\rangle = \sum_k a_k |e_k\rangle$ . The probe register is prepared in the state  $|\psi(0)\rangle = (|0\rangle + |-1\rangle)/\sqrt{2}$  (see Methods).

In the next step, a controlled- $U(t)$  gate for different times  $t$ , where  $U(t) = \exp(-iH_{\text{sim}}t)$ , is applied to encode the energies into a relative phase, resulting in the state

$$|\psi(t)\rangle = \frac{1}{\sqrt{2}} \sum_k a_k (|0\rangle + e^{-iE_k t} |-1\rangle) |e_k\rangle. \quad (2)$$

The reduced density matrix of the probe register,

$$\rho_{\text{probe}}(t) = \frac{1}{2} \begin{pmatrix} 1 & \sum_k |a_k|^2 e^{-iE_k t} \\ \sum_k |a_k|^2 e^{iE_k t} & 1 \end{pmatrix}, \quad (3)$$

contains the information about the energies in its off-diagonal elements. This information is then transferred to the electron spin for readout by a nuclear spin  $\frac{\pi}{2}$ -pulse and selective  $\pi$ -pulses on the electron spin-1 (Fig. 2a).

To measure the energy precisely, we perform classical Fourier analysis on the signal for different times  $(t_s, 2t_s, \dots, Lt_s)$ . This readout method can help to resolve the probability  $|a_k|^2$  of each eigenstate  $|e_k\rangle$  and approximate the corresponding energy  $E_k$ . We choose  $t_s$  such that the sampling rate  $\frac{1}{t_s} > |E_n|/\pi$ . To enhance the precision of the energy eigenvalues, an iterative phase estimation algorithm is performed. A central feature of this algorithm includes repeating the unitary operator  $U$  to increase readout precision. Expressing the energy as a string of decimal digits,  $E_k = x_1.x_2x_3\dots$ , the first digit  $x_1$  can be determined by the first round phase estimation process. Once  $x_1$  is known, the second digit  $x_2$  can be iteratively determined by implementing the unitary operator  $U^p$ , where  $p = 10$ . For the  $k^{\text{th}}$  iteration,  $p = 10^{k-1}$ .

An increasingly precise energy can be obtained through continued iterations. However, the repetitions and therefore the iterations are fundamentally limited by the coherence time of the quantum system. Moreover, the accumulated gate errors become a dominant limitation of the energy precision as the repetitions increase. To avoid such shortcomings, the time evolution operators  $U^p$  are realized and optimized with optimal control theory (see Methods). The precision we reach in our experiments demonstrates that optimal control can overcome several difficult features found when scaling up the register size [36]. Although it cannot be applied in large registers to generate the quantum gates directly, it can be used to generate flexible smaller building blocks, ensuring high-fidelity control in future large scale applications. In the present case, the method is unscalable because we compute the unitary propagator using a classical computer. However, by using a Trotter-type gate sequence to implement the propagators, e.g. [17], this can be designed with polynomially scaling.

Fig. 2b shows our results of internuclear distance  $R = 90$  pm with trial state  $|+1\rangle$ . The position of the peak indicates the eigenvalue of molecular Hamiltonian with an offset  $\text{tr}(H_{\text{sim}})/3$ . The Fourier spectrum has only one major peak, which shows that the trial state  $|+1\rangle$  is close to the ground state. As the iterations increase, more precise decimal digits of the ground state energy are resolved. After 13 repetitions the molecular energy is extracted to be  $-1.020170538763387 \pm 8 \times 10^{-15}$  Hartree, very close to the theoretic value, which is  $-1.020170538763381$  Hartree, with an uncertainty of  $\pm 1.4 \times 10^{-14}$  Hartree.

Once the energies have been measured, we can obtain the potential energy surface of the molecule by repeating the procedure for different distances  $R$  (see Fig. 3). The ground state energy surface is obtained with trial state  $|+1\rangle$  and first excited state energy surface is obtained with trial state  $|-1\rangle$ . We obtain the remaining eigenenergy (of the second excited state) without further measurement by subtracting the ground and first excited state energies from the trace of  $H_{\text{sim}}$ . The potential energy surfaces can be used to compute key molecular properties such as ionization energies and vibrational energy levels. An important example is the equilibrium geometry: we found the minimal energy for the ground state,  $-2.86269$  Hartree, at a bond length of 91.3 pm. In addition, we obtained a binding energy of 0.07738 Hartree in our basis. To improve the accuracy of our results we would need to simulate the system in a larger basis, thereby requiring more qutrits.

## DISCUSSION

We will now briefly discuss several of the implications of this study. Current quantum simulations cannot outperform classical devices. In large systems, the simulated propagators can be implemented using Trotter sequences and should be accompanied by error correction. Optimal control methods, as we have demonstrated here, should prove necessary to perform these tasks with satisfactory precision. We have demonstrated the most precise quantum simulation of molecular energies to date, which represents an important step towards the advanced level of control required by future quantum simulators that will outperform classical methods. The energies we obtained for the helium hydride cation surpass chemical precision by 10 orders of magnitude (with respect to the basis). The accuracy of our results can be increased by using a larger, more flexible single-particle basis set but this will require a larger quantum simulator that eventually will require error correction schemes [19].

Our study presents evidence that quantum simulators can be controlled well enough to recover increasingly precise data. The availability of highly accurate energy eigenvalues of large molecules is presently far out of reach of existing computational technology, and quantum sim-

ulation could open the door to a vast range of new technological applications. The approach we took was based on iterative phase estimation [46] and optimal control decompositions [36]—these will form key building blocks for any solid-state quantum simulator. Even more generally, this study would suggest that the techniques presented here should be employed in any future simulator that will outperform classical simulations of electronic structure calculations.

## ACKNOWLEDGEMENTS

V.B. and J.D.B. acknowledge financial support by Fondazione Compagnia di San Paolo through the Q-ARACNE project. J.D.B. would also like to acknowledge the Foundational Questions Institute (under grant FQXi-RFP3-1322) for financial support. R.B. and A.A.-G. acknowledge support from the Air Force Office of Scientific Research under contract FA9550-12-1-0046, as well as the National Science Foundation CHE-1152291 and the Corning Foundation. J.W. acknowledges support by the EU via IP SIQS and the ERC grant SQUTEC as well as the DFG via the research group 1493 and SFB/TR21 and the Max Planck Society. J.D.W. thanks the VCQ and Ford postdoctoral fellowships for support. We thank Mauro Faccin and Jacob Turner for providing valuable feedback regarding the manuscript.

---

\* jacob.biamonte@qubit.org

† j.wrachtrup@physik.uni-stuttgart.de

- [1] R. P. Feynman, *Int. J. Theor. Phys.* **21**, 467 (1982).
- [2] S. Lloyd, *Science* **273**, 1073 (1996).
- [3] S. Wiesner, “Simulations of many-body quantum systems by a quantum computer,” (1996), arXiv:quant-ph/9603028.
- [4] C. Zalka, *Fortschritte der Physik* **46**, 877 (1998).
- [5] D. S. Abrams and S. Lloyd, *Phys. Rev. Lett.* **79**, 2586 (1997).
- [6] D. W. Berry, G. Ahokas, R. Cleve, and B. C. Sanders, *Communications In Mathematical Physics* **270**, 359 (2007).
- [7] I. Georgescu, S. E. Brown, and V. A. Mandelshtam, *J. Chem. Phys.* **138**, 134502 (2013).
- [8] A. Trabesinger, *Nature Physics Insight: Quantum Simulation* **8**, 263 (2012).
- [9] M.-H. Yung, J. D. Whitfield, S. Boixo, D. G. Tempe, and A. Aspuru-Guzik, in *Quantum Information and Computation for Chemistry*, *Advances in Chemical Physics*, Vol. 154 (John Wiley & Sons, Inc., 2014) pp. 67–106, arXiv:1203.1331.
- [10] I. Kassal, J. D. Whitfield, A. Perdomo-Ortiz, M.-H. Yung, and A. Aspuru-Guzik, *Ann. Rev. Phys. Chem.* **62**, 185 (2011).
- [11] K. L. Brown, W. J. Munro, and V. M. Kendon, *Entropy* **12**, 2268 (2010).

- [12] D. Lu, B. Xu, N. Xu, Z. Li, H. Chen, X. Peng, R. Xu, and J. Du, *Phys. Chem. Chem. Phys.* **14**, 9411 (2012).
- [13] I. M. Georgescu, S. Ashhab, and F. Nori, *Rev. Mod. Phys.* **86**, 153 (2014), arXiv:1308.6253.
- [14] T. H. Johnson, S. R. Clark, and D. Jaksch, arXiv preprint (2014).
- [15] A. Aspuru-Guzik, A. D. Dutoi, P. J. Love, and M. Head-Gordon, *Science* **309**, 1704 (2005), arXiv:quant-ph/0604193.
- [16] B. P. Lanyon, J. D. Whitfield, G. G. Gillet, M. E. Goggin, M. P. Almeida, I. Kassal, J. D. Biamonte, M. Mohseni, B. J. Powell, M. Barbieri, A. Aspuru-Guzik, and A. G. White, *Nature Chemistry* **2**, 106 (2010), arXiv:0905.0887.
- [17] J. D. Whitfield, J. Biamonte, and A. Aspuru-Guzik, *Mol. Phys.* **2**, 106 (2010), 1001.3855.
- [18] I. Kassal, J. D. Whitfield, A. Perdomo-Ortiz, M.-H. Yung, and A. Aspuru-Guzik, *Annu. Rev. Phys. Chem.* **62**, 185 (2010).
- [19] N. Cody Jones, J. D. Whitfield, P. L. McMahon, M.-H. Yung, R. V. Meter, A. Aspuru-Guzik, and Y. Yamamoto, *New Journal of Physics* **14**, 115023(1) (2012).
- [20] D. Wecker, B. Bauer, B. K. Clark, M. B. Hastings, and M. Troyer, “Can quantum chemistry be performed on a small quantum computer?” (2013), arXiv:1312.1695.
- [21] B. Toloui and P. J. Love, “Quantum algorithms for quantum chemistry based on the sparsity of the CI-matrix,” (2013), arXiv:1312.2579.
- [22] M. B. Hastings, D. Wecker, B. Bauer, and M. Troyer, “Improving quantum algorithms for quantum chemistry,” (2014), arXiv:1403.1539.
- [23] A. Y. Kitaev, A. H. Shen, and M. N. Vyalıy, *Classical and Quantum Computation*, Graduate Studies in Mathematics, Vol. 47 (American Mathematical Society, 2002).
- [24] G. Puentes, G. Waldherr, P. Neumann, G. Balasubramanian, and J. Wrachtrup, *Sci Rep* **4**, 4677 (2014).
- [25] J. Du, N. Xu, X. Peng, P. Wang, S. Wu, and D. Lu, *Phys. Rev. Lett.* **104**, 030502 (2010).
- [26] D. Lu, N. Xu, R. Xu, H. Chen, J. Gong, X. Peng, and J. Du, *Phys. Rev. Lett.* **107**, 020501 (2011).
- [27] A. Peruzzo, J. McClean, P. Shadbolt, M.-H. Yung, X.-Q. Zhou, P. J. Love, A. Aspuru-Guzik, and J. L. O’Brien, “A variational eigenvalue solver on a quantum processor,” (2013), arXiv:1304.3061.
- [28] A. Gruber, A. Dräbenstedt, C. Tietz, L. Fleury, J. Wrachtrup, and C. von Borczyskowski, *Science* **276**, 2012 (1997).
- [29] P. Neumann, J. Beck, M. Steiner, F. Rempp, H. Fedder, P. R. Hemmer, J. Wrachtrup, and F. Jelezko, *Science* **329**, 542 (2010).
- [30] L. Robledo, L. Childress, H. Bernien, B. Hensen, P. F. a. Alkemade, and R. Hanson, *Nature* **477**, 574 (2011).
- [31] G. Waldherr, Y. Wang, S. Zaiser, M. Jamali, T. Schulte-Herbrüggen, H. Abe, T. Ohshima, J. Isoya, J. F. Du, P. Neumann, and J. Wrachtrup, *Nature* **506**, 204 (2014).
- [32] P. Neumann, N. Mizuochi, F. Rempp, P. Hemmer, H. Watanabe, S. Yamasaki, V. Jacques, T. Gaebel, F. Jelezko, and J. Wrachtrup, *Science* **320**, 1326 (2008).
- [33] E. Togan, Y. Chu, A. S. Trifonov, L. Jiang, J. Maze, L. Childress, M. V. G. Dutt, A. S. Sorensen, P. R. Hemmer, A. S. Zibrov, and M. D. Lukin, *Nature* **466**, 730 (2010).
- [34] F. Dolde, I. Jakobi, B. Naydenov, N. Zhao, S. Pezzagna, C. Trautmann, J. Meijer, P. Neumann, F. Jelezko, and J. Wrachtrup, *Nature Phys.* **8**, 1 (2013).
- [35] H. Bernien, B. Hensen, W. Pfaff, G. Koolstra, M. S. Blok, L. Robledo, T. H. Taminiau, M. Markham, D. J. Twitchen, L. Childress, and R. Hanson, *Nature* **497**, 86 (2013).
- [36] F. Dolde, V. Bergholm, Y. Wang, I. Jakobi, B. Naydenov, S. Pezzagna, J. Meijer, F. Jelezko, P. Neumann, T. Schulte-Herbrüggen, J. Biamonte, and J. Wrachtrup, *Nature Communications* **5**, 3371 (2014), arXiv:1309.4430.
- [37] T. H. Taminiau, J. Cramer, T. van der Sar, V. V. Dobrovitski, and R. Hanson, *Nature Nanotechnology* , 1 (2014).
- [38] G. Balasubramanian, P. Neumann, D. Twitchen, M. Markham, R. Kolesov, N. Mizuochi, J. Isoya, J. Achard, J. Beck, J. Tessler, V. Jacques, P. R. Hemmer, F. Jelezko, and J. Wrachtrup, *Nature materials* **8**, 383 (2009).
- [39] P. C. Maurer, G. Kucsko, C. Latta, L. Jiang, N. Y. Yao, S. D. Bennett, F. Pastawski, D. Hunger, N. Chisholm, M. Markham, D. J. Twitchen, J. I. Cirac, and M. D. Lukin, *Science* **336**, 1283 (2012).
- [40] F. Jelezko, T. Gaebel, I. Popa, M. Domhan, A. Gruber, and J. Wrachtrup, *Phys. Rev. Lett.* **93**, 130501 (2004).
- [41] M. V. G. Dutt, L. Childress, L. Jiang, E. Togan, J. Maze, F. Jelezko, A. S. Zibrov, P. R. Hemmer, and M. D. Lukin, *Science* **316**, 1312 (2007).
- [42] J. M. Taylor, P. Cappellaro, L. Childress, L. Jiang, D. Budker, P. R. Hemmer, A. Yacoby, R. Walsworth, and M. D. Lukin, *Nature Physics* **4**, 29 (2008).
- [43] M. W. Doherty, V. V. Struzhkin, D. A. Simpson, L. P. McGuinness, Y. Meng, A. Stacey, T. J. Karle, R. J. Hemley, N. B. Manson, L. Hollenberg Lloyd C., and S. Praver, *Phys. Rev. Lett.* **112**, 47601 (2014).
- [44] A. Bermudez, F. Jelezko, M. B. Plenio, and A. Retzker, *Phys. Rev. Lett.* **107**, 150503 (2011).
- [45] E. A. Engel, N. Doss, G. J. Harris, and J. Tennyson, *Mon. Not. R. Astron. Soc.* **357**, 471 (2005).
- [46] S. Parker and M. B. Plenio, *Phys. Rev. Lett.* **85**, 3049 (2000).
- [47] J. D. Biamonte, V. Bergholm, J. D. Whitfield, J. Fitzsimons, and A. Aspuru-Guzik, *AIP Advances* **1**, 022126 (2011), arXiv:1002.0368.
- [48] W. J. Hehre, R. F. Stewart, and J. A. Pople, *J. Chem. Phys.* **51**, 2657 (1969).
- [49] T. D. Crawford, C. D. Sherrill, E. F. Valeev, J. T. Fermann, R. A. King, M. L. Leininger, S. T. Brown, C. L. Janssen, E. T. Seidl, J. P. Kenny, and W. D. Allen, *Journal of Computational Chemistry* **28**, 1610 (2007).
- [50] N. Khaneja, T. Reiss, C. Kehlet, T. Schulte-Herbrüggen, and S. J. Glaser, *J. Mag. Res.* **172**, 296 (2005).
- [51] Z. Zimborás, M. Faccin, Z. Kádár, J. D. Whitfield, B. P. Lanyon, and J. Biamonte, *Scientific Reports* **3**, 2361 (2013).

## Methods

### Computation of molecular Hamiltonians

The full configuration interaction Hamiltonian is a sparse matrix and each matrix element can be computed in polynomial time. The  $N$ -electron Hamiltonian is asymptotically sparse. For a basis set with  $M$  orbitals, there are  $M^4$  terms in the Hamiltonian but the Hamiltonian is of size  $\frac{M!}{N!(M-N)!} \approx M^N$  which is exponential as the number of electrons grow. To generate the Hamiltonian, we fix the nuclear configuration and then compute the necessary one- and two-body integrals which parameterize the FCI matrix at each fixed bond length in the standard STO-3G basis [48], using the PSI3 electronic structure package [49]. The minimal basis HeH<sup>+</sup> system has two spatial orbitals which we denote as  $g(r)$  and  $e(r)$  and two spin functions denoted as  $\alpha(\sigma)$  and  $\beta(\sigma)$  which are eigenstates of the  $S_z$  operator. We combine these to form four spin orbitals,  $\chi_1 = g(r)\alpha(\sigma)$ ,  $\chi_2 = g(r)\beta(\sigma)$ ,  $\chi_3 = e(r)\alpha(\sigma)$  and  $\chi_4 = e(r)\beta(\sigma)$ . There are six possible two-electron Slater determinants,  $\Psi_1 = \mathcal{A}(\chi_1\chi_2)$ ,  $\Psi_2 = \mathcal{A}(\chi_1\chi_3)$ ,  $\Psi_3 = \mathcal{A}(\chi_1\chi_4)$ ,  $\Psi_4 = \mathcal{A}(\chi_2\chi_3)$ ,  $\Psi_5 = \mathcal{A}(\chi_2\chi_4)$ , and  $\Psi_6 = \mathcal{A}(\chi_3\chi_4)$ . More explicitly,

$$\mathcal{A}(\chi_i\chi_j) = \frac{1}{\sqrt{2}} \begin{vmatrix} \chi_i(r_1\sigma_1) & \chi_j(r_1\sigma_1) \\ \chi_i(r_2\sigma_2) & \chi_j(r_2\sigma_2) \end{vmatrix}. \quad (4)$$

States  $\Psi_1$ ,  $\Psi_3$ ,  $\Psi_4$ , and  $\Psi_6$  have total projected spin of  $M_z = 0$  whereas  $\Psi_2$  and  $\Psi_5$  have projected values of  $M_z = 1$  and  $M_z = -1$  respectively. Only  $\Psi_1$  and  $\Psi_6$  are valid eigenstates of the total spin operator  $S^2$ ; however, the symmetric and antisymmetric combinations of  $\Psi_3$  and  $\Psi_4$  yield the  $m_s = 0$  triplet and an additional singlet, respectively. When a computation is requested on the singlet state, the PSI3 package computes the symmetry-adapted FCI matrix in the basis of  $\Psi_1$ ,  $\Psi_3$ ,  $\Psi_4$  and  $\Psi_6$ . By combining  $\Psi_3$  and  $\Psi_4$  we obtained the three HeH<sup>+</sup> singlet states used in this experiment:  $\Psi_1$ ,  $\Psi_6$  and  $\frac{1}{\sqrt{2}}(\Psi_3 - \Psi_4)$ .

### Sample characteristics

We use a nitrogen-vacancy center in high-purity diamond grown by microwave-assisted chemical vapor deposition (CVD). The intrinsic nitrogen content of the grown crystal is below 1 ppb and the <sup>12</sup>C content is enriched to 99.9%. Experiments are performed at room temperature with an applied magnetic field of 11 gauss. The electron spin's coherence times are  $T_2^* \approx 80 \mu\text{s}$  and  $T_2 \approx 600 \mu\text{s}$ .

### NV system

In a magnetic field  $B_0$  aligned along the NV symmetry axis, the electronic and nuclear spin system has the Hamiltonian

$$H/\hbar = 2\pi\Delta S_z^2 + \gamma_e B_0 S_z + 2\pi A_{\text{hf}} S_z I_z + 2\pi Q I_z^2 + \gamma_N B_0 I_z$$

where  $S_z$  and  $I_z$  are the dimensionless spin-1 operators for the electrons and the <sup>14</sup>N nucleus, respectively.  $\Delta \approx 2.87$  GHz and  $Q \approx -4.94$  MHz are the zero-field splitting of the electronic spin and quadrupole splitting of the nuclear spin. The hyperfine coupling coefficient is  $A_{\text{hf}} \approx 2.16$  MHz. The Larmor frequencies are defined as  $\omega_i := \gamma_i B_0$ , where  $\gamma_i$  is the gyromagnetic ratio of the spin (electronic or nuclear).

### System initialization

In the experiment, the <sup>14</sup>N nuclear spin is initially in a thermal state. It is polarized into the spin state  $|m_I = 0\rangle$  by means of optical pumping of the electron spin followed polarization transfer realized with electron spin and nuclear spin control (see Fig. 4). The second short laser pulse repolarizes the electron spin into  $|m_s = 0\rangle$ , leaving the spins in the state  $|m_s = 0, m_I = 0\rangle$  [41]. In practice, the imperfect control and short  $T_1 \approx 1.9 \mu\text{s}$  time of nuclear spin under laser illumination will result in imperfect polarization of the nuclear spin. To enhance the polarization effect, we repeat the process two times and tune the second laser pulse to an optimal length around 300 ns. The observed electron spin Rabi oscillation in the  $m_I = 0$  subspace indicates a final polarization of around 60%. After the polarization process,

the electron spin is then prepared into the  $|m_s = +1\rangle$  or  $|m_s = -1\rangle$  state by another microwave  $\pi$  pulse unconditional on the nuclear spin state. Note that only the phase of the nuclear spin superposition state contains information in the IPEA process, therefore imperfect polarization would not affect the accuracy of final energy measurement.

### Controlled $U(t)$ gate realization

In the experiment, every individual controlled gate  $U' = (e^{-iH_{\text{sim}}t})^p$  can be realized by decomposing it into more basic but highly complicated microwave pulses. However, this approach will accumulate considerable control errors. To avoid such shortcomings, we use an alternative method, optimal control, which has recently been used to achieve high-fidelity control in coupled NV centers in diamond [36].

To make the calculation feasible, another equivalent controlled gate  $U^* = e^{-iH't}$  with the Hamiltonian  $H' = H_{\text{sim}} - \text{tr}(H_{\text{sim}})/3$  is calculated. This operation will only introduce additional  $O(1)$  complexity. One then needs to add this constant value  $\text{tr}(H_{\text{sim}})/3$  back to the final measured energies.

To calculate  $U^*$ , we use the GRAPE algorithm [50] to optimize the pulse sequence, with the final fidelity always larger than 0.99. For every controlled gate, the pulse sequence consists of 10 pieces of 140 ns each. Two microwave frequencies are applied simultaneously to control the electron spin, in the observed hyperfine peaks of the  $|m_I = -1, m_s = 0\rangle \rightarrow |m_I = -1, m_s = +1\rangle$  and  $|m_I = -1, m_s = 0\rangle \rightarrow |m_I = -1, m_s = -1\rangle$  transitions. More details about the optimal control method can be found in reference [36].

### A symmetry of the ground state energy problem

If we write the system Hamiltonian as  $H = T + K$  where diagonal  $T$  accounts for the HF approximations and off-diagonal  $K$  accounts from the Born-Oppenheimer approximate treatment of the problem. We note that whenever the support of  $K$  corresponds to the adjacency matrix of a bipartite graph, then  $H = T + K$  and  $L = T - K$  are cospectral. This follows from the proof [51] that any bipartite (necessarily time-inversion symmetric) Hamiltonian  $H$  is on the same orbit as  $-H$  under conjugation by diagonal unitarians (e.g. there exists a diagonal unitary  $\Lambda$  such that  $\Lambda H \Lambda^\dagger = -H$ ) where  $T$  is central under this action. Hence, they represent the same ground-state energy problems, providing an equivalent problem instance  $L$  to attempt state preparation on. It turns out that all of the quantum chemistry algorithms realized to date [16, 25, 26] have this property including our own demonstration, where the underlying graph corresponds to a tree. This observation provides a second benchmark to be considered in future experiments.

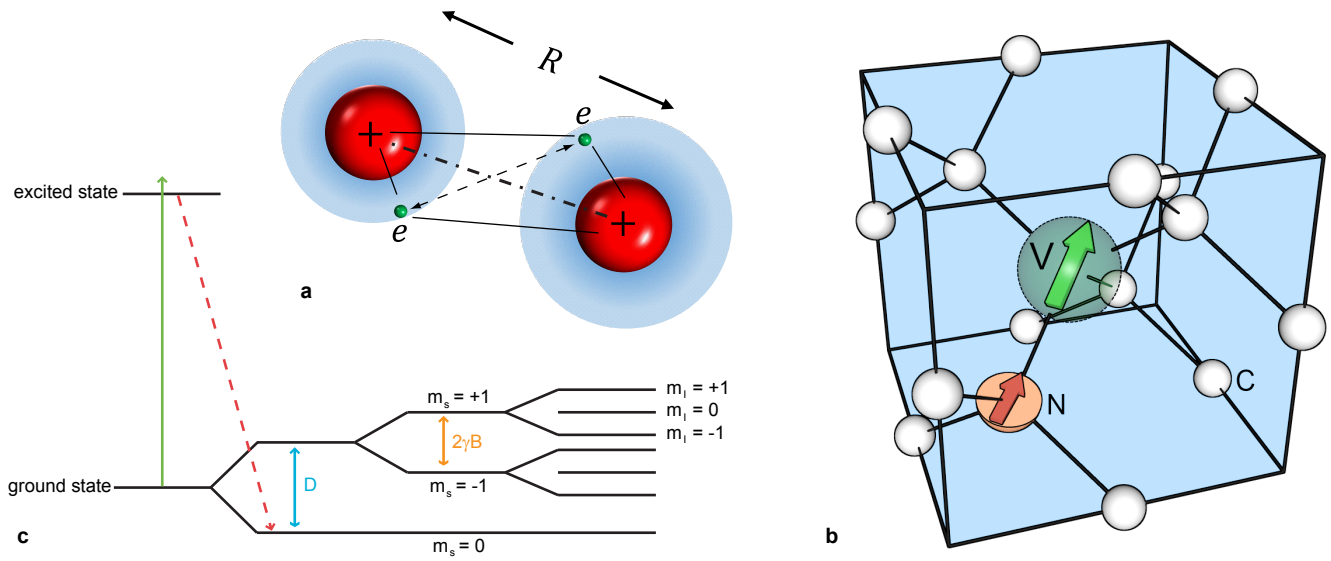


Figure 1. **Calculation of  $\text{HeH}^+$  molecular energy with NV spin register in diamond** (a)  $\text{HeH}^+$ , molecule to be simulated. It consists of a hydrogen and a helium nucleus, and two electrons. The distance (bond length) between the nuclei is denoted by  $R$ . Dot-dashed line, straight line, and dotted arrow indicate the nucleus-nucleus, electron-nucleus and electron-electron Coulomb interactions, respectively. (b) A nitrogen-vacancy center in diamond, used as a quantum simulator. The electron spin is used for simulation and the nuclear spin as the probe qubit for energy readout. (c) Energy level diagram for the coupled spin system formed by the NV electron spin and nearby  $^{14}\text{N}$  nuclear spin. Optical transitions between ground and excited state are used to initialize and measure the electron spin state.

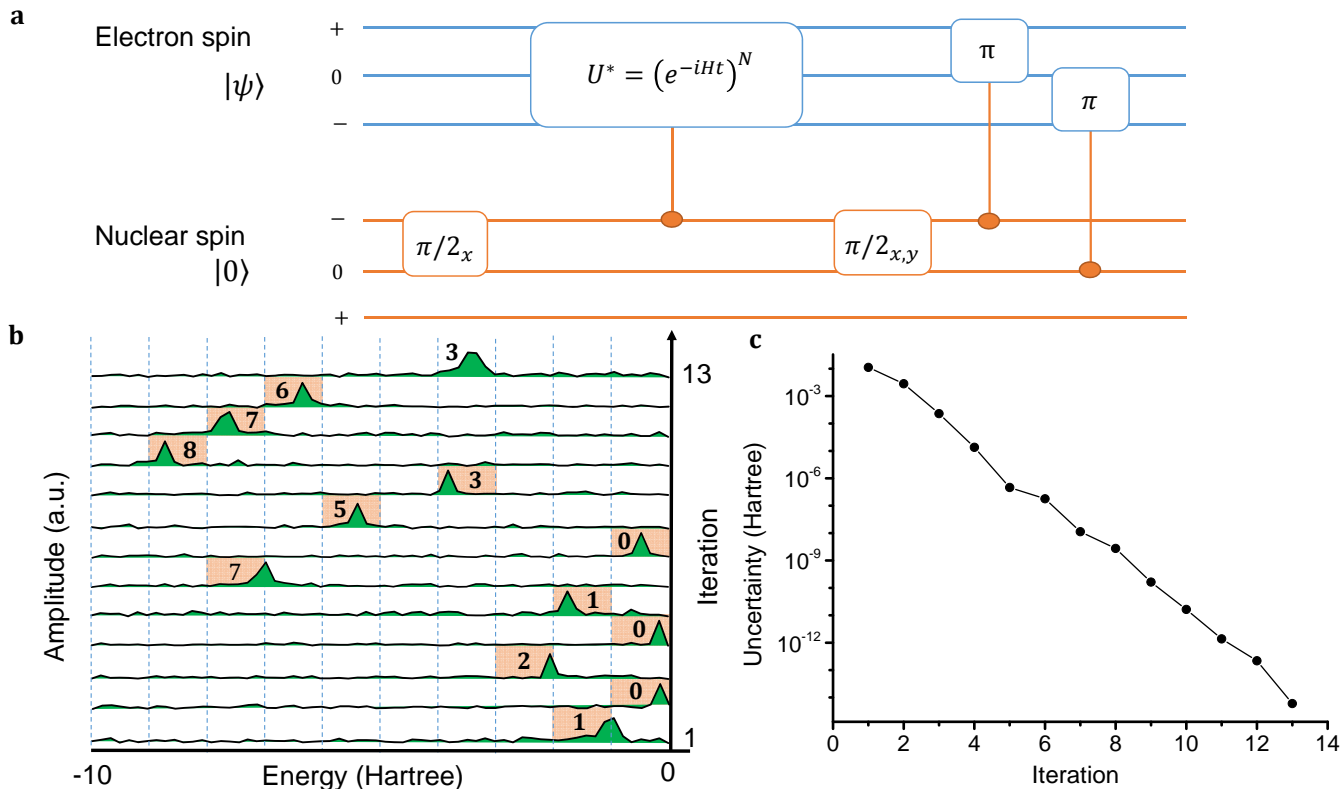


Figure 2. **Energy readout through quantum phase estimation algorithm** (a) Experimental implementation of the IPEA algorithm. The controlled gate  $U^*$  is realized using optimal control (see Methods). The  $x, y$  phases in the last  $\pi/2$  pulse measure the real and imaginary parts of the signal, respectively, which yield the sign of the measured energy. The number of repetitions  $N = 10^{k-1}$  depends on the iteration  $k$ . (b) Experimental results of iterative phase estimation algorithm to enhance the precision of measured energy for the case of  $R = 0.9$ . The Fourier spectrum of the first iteration ( $k = 1$ ) fixes the energy roughly between  $-10$  and  $0$  Hartree. The precision is then improved iteratively by narrowing down the energy range. In each iteration, the energy range is divided into ten equal segments. The red area indicates the energy range for the next iteration. After each iteration at least one decimal digit, denoted by the number in the red area, is resolved. (c) The uncertainty of the measured energy as a function of the iteration number.

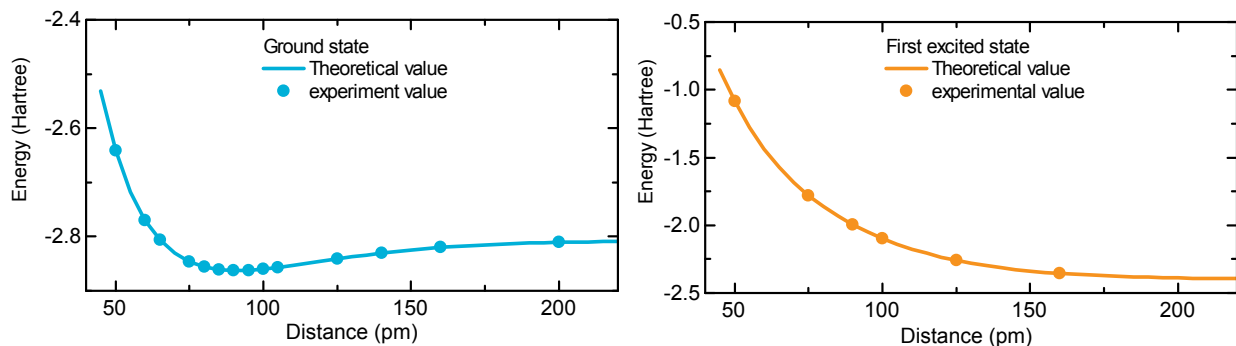


Figure 3. **Energy surfaces of the  $\text{HeH}^+$  molecule.** The energy surface of the second excited state can be obtained by subtracting energies of the the ground and first excited states from the trace of  $H_{\text{sim}}$ , and is not shown. All the measured energies are obtained in five iterations.

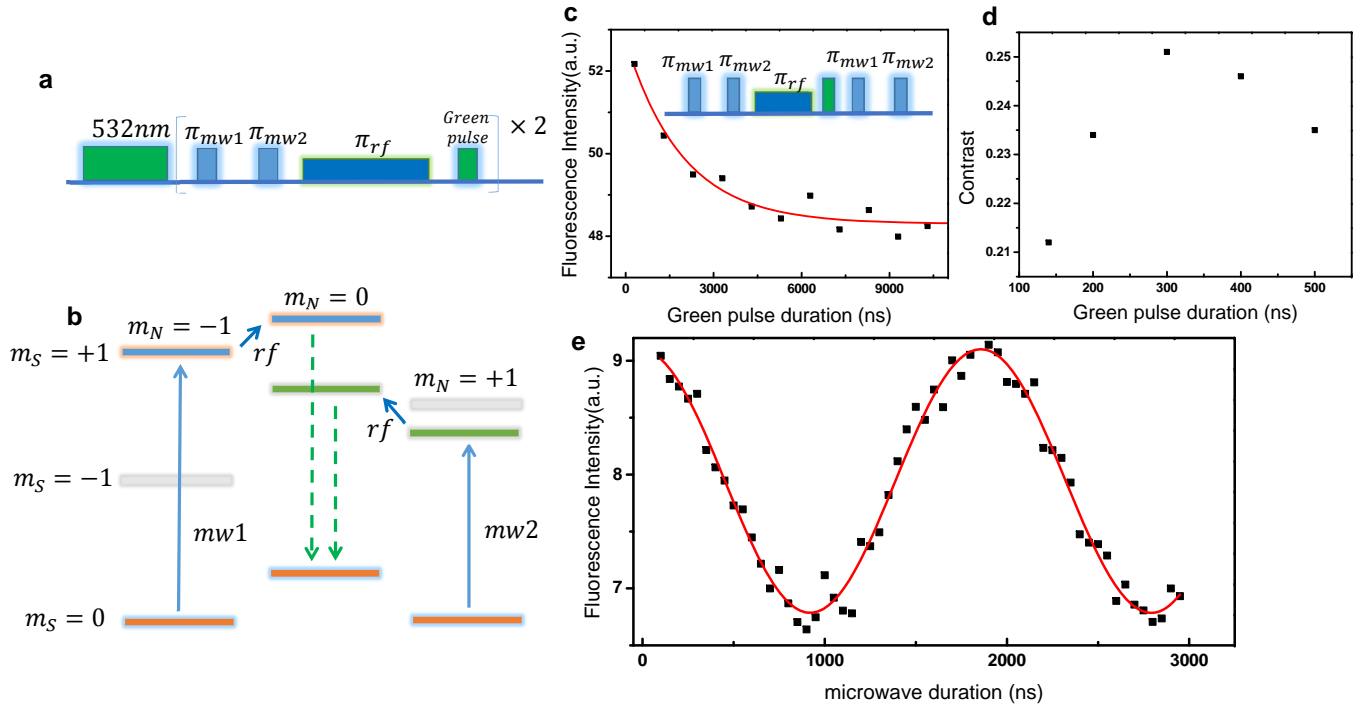


Figure 4. **Polarization of  $^{14}\text{N}$  nuclear spin.** (a) Experimental pulse sequence to polarize the  $^{14}\text{N}$  nuclear spin. (b) Dynamical process during one polarization step. (c) Initialization decay of nuclear spin under laser illumination. The fit (red line) shows an exponential decay with time constant  $1.9 \pm 0.3 \mu\text{s}$ . The pulse sequence is shown in the inset. (d) The contrast of electron spin Rabi oscillation in the  $m_N = 0$  subspace (here: a measure for the degree of nuclear spin initialization) varies with the second laser pulse length. (e) The electron spin Rabi oscillation in the  $m_N = 0$  subspace for 300 ns green pulse duration.